Recovering precious metals from spent catalysts by peroxydisulfate-based advanced oxidation process

Chengliang Xiao (xiaoc@zju.edu.cn)
College of Chemical and Biological Engineering, Zhejiang University
Anting Ding
College of Chemical and Biological Engineering, Zhejiang University
Ming Li
Institute of Zhejiang University-Quzhou
Chuanying Liu
Institute of Zhejiang University - Quzhou
Qibin Yan
College of Chemical and Biological Engineering, Zhejiang University
Lecheng Lei
Zhejiang University https://orcid.org/0000-0002-4471-5898

Article

Keywords:

Posted Date: July 25th, 2023

DOI: https://doi.org/10.21203/rs.3.rs-3181647/v1

Additional Declarations: There is **NO** Competing Interest.

Recovering precious metals from spent catalysts by peroxydisulfate-based advanced oxidation process

Anting Ding,[a,b] Ming Li,[b] Chuanying Liu,[b] Qibin Yan,[a] Lecheng Lei,[a,b] and Chengliang Xiao[a,b,*]

[a] College of Chemical and Biological Engineering, Zhejiang University, Hangzhou 310058, China

[b] Institute of Zhejiang University-Quzhou, Quzhou 324000, China

*Chengliang Xiao

Email: xiaoc@zju.edu.cn

Abstract

The recovery of precious metals from discarded wastes is an attractive potential remedy for their supply disruption risk. Nevertheless, the use of conventional solvents in metallurgical processes has significant negative environmental effects. Here, we report peroxydisulfate (PDS)-based advanced oxidation process (AOPs) to develop a novel and efficient leaching process for recovering precious metals from spent catalysts. The PDS/NaCl photochemical system could fully dissolve palladium (Pd) and gold (Au) in 300 min. By introducing Fe(II), the PDS/$FeCl_2 \cdot 4H_2O$ solution functioned as Fenton-like system, which enhanced the leaching efficiency and required no xenon (Xe) lamp light irradiation. Electron paramagnetic resonance (EPR) and ^{18}O isotope tracing experiments revealed the reactive oxidation species of $SO_4^{\cdot -}$, ·OH and Fe(IV)=O were responsible for the oxidative dissolution of precious metals. Density functional theory calculations showed that the total energy barrier for the three species were 7.62, 18.46 and 17.52 kcal mol^{-1}, respectively. Solvent leaching and one-step electrodeposition recovered high-purity precious metals and maintained solvent dissolution and electrochemical stability after 5 cycles. Strong acids, poisonous cyanide, volatile organic solvents, light irradiation, and photocatalysts were not used during recovery. This work will enable a green and

sustainable precious metal recovery approach and encourage AOPs technology for secondary resource recycling.

Introduction

As representative precious metals (PMs), gold (Au) and silver (Ag) have been treasured since ancient times for their beauty and performance. They emerged as essential metals in electrical industries in the late 20th century because of their superior electrical conductivity, corrosion resistance, and other desirable combinations of physical and chemical properties[1-3]. From 2010 to 2022, the global gold mine reserves have remained relatively stable. In 2022, global gold reserves were 52,000 metric tons, down from a peak of 57,000 metric tons in 2016. According to data from the World Gold Council, the demand for gold globally originates from diverse fields, including jewelry and technology, reached 4706 metric tons in 2022. However, only about 24% of the global demand for gold is recovered from secondary resources containing gold. Most of the gold supply depends on gold mining[4]. Thus, recovering gold from secondary resources to decrease the supply risk is essential[5-7]. Additionally, platinum group metals (PGMs), such as platinum (Pt), palladium (Pd), and rhodium (Rh) which are rare PMs with high economic values, are often applied in automobile three-way catalysts[8,9]. With the swift improvement of products, the demand for PMs is increasing, but the supply is insufficient. Electronic waste (e-waste) and waste catalysts are the primary secondary resources of PMs, which account for the majority of the market[10,11].

Unfortunately, mining and capturing PMs from ores, catalysts, and e-waste is a significant challenge. There are two primary steps involved in the process of recovering PMs. The first step is the leaching of PM^0 into PM^{x+} solutions, followed by the conversion of PM^{x+} to PM^0 from leachate. The first recovery step involving oxidation process is the most difficult due to the insoluble nature of PMs[12,13]. Aqua regia, which is highly corrosive and toxic, and cyanidation are extensively used dissolution techniques in the industry, endangering the environment[14-18]. Therefore, various new solvents have been developed for recovering PMs. For example, Lin and colleagues[19] created “organic aqua regia” by combining thionyl chloride with some organic solvents like N, N-dimethylformamide, pyridine, or imidazole to dissolve PMs. Additionally, dimethylformamide containing liquid chloride was utilized to leach Pt[12].

Advanced oxidation processes (AOPs) involve producing radicals with high oxidization ability for the degradation or transformation of pollutants[20-24]. In recent years, the strong oxidizing radicals generated during AOPs have been utilized to achieve the oxidative dissolution of PMs. For example, under the irradiation of ultraviolet (UV) light, Li et al. were able to transform Au nanoparticles into cyanide gold oligomers by using a mixture consisting of acetonitrile (CH_3CN) and benzaldehyde (C_7H_6O)[25]. Electron paramagnetic resonance (EPR) was used to demonstrate that ·CN and ·OH radicals in CH_3CN and C_7H_6O, respectively, were active species that were capable of dissolving Ag, Pd, and Pt. Chen et al. used a mixture of CH_3CN and dichloromethane (CH_2Cl_2) to successfully oxidize and dissolve seven PMs (Ag, Au, Pd, Pt, Ru, Rh, and Ir) under light conditions and used TiO_2 photocatalysts to assist in generating CH_2CN·, $CHCl_2$·, and O_2·$^-$ radicals[10]. However, organic solvents like C_7H_6O, CH_3CN, and CH_2Cl_2 are not considered environmental-friendly chemicals. Moreover, given the production of considerable volumes of secondary waste as well as the emission of volatile toxic gases, these methods provide a serious risk to the environment.

The development of peroxydisulfate (PDS)-based advanced oxidation process (AOPs) has attracted increasing attention from the academic and industrial communities. PDS is the precursor of sulfate (SO_4·$^-$) or hydroxyl (·OH) radicals activated using heat, transition metals, ultrasonic, and light radiations[26-30]. To the best of our knowledge, there has been no report on recovering PMs using highly reactive radicals generated from PDS thus far. Therefore, we take advantage of highly reactive species generated from PDS-based AOPs to develop a novel and simple leaching process. The PDS/NaCl photochemical solvent and the enhanced Fenton-like system of PDS/$FeCl_2$·$4H_2O$ solution serve as powerful green solvents to recover PMs without strong acids, volatile organic solvents, light irradiation and photocatalysts. PMs were successfully recovered from their individual waste catalysts of Pd and Au via PDS/$FeCl_2$·$4H_2O$ solution dissolution and electrodeposition. It potentially offers a green and sustainable approach to recovering PMs and is anticipated that it will inspire additional efforts to the advancement of AOPs technologies for resource recycling.

Results

Dissolution properties of PDS/NaCl photochemical system. The cleavage of the peroxide bond in the PDS molecule (see **Fig. 1a** for its structure), which takes place via

energy and electron transfer processes, results in the production of highly reactive $SO_4^{\cdot -}$. PMs leaching systems require both strong oxidation and coordination capabilities[31-33]. Therefore, PDS combined with the most common salt NaCl was chosen to form a new solvent for the leaching of PMs because chlorine ions (Cl^-) have a strong ability in an aqueous solution[34]. As schematically illustrated in **Fig. 1b**, PMs were mixed in the solution of PDS and NaCl under xenon (Xe) lamp light. The color was rapidly changed and deepened over time in this photochemical system (**Fig. 1c**). Pt, Rh, Pd, Au, and Ag, which are the five common PMs in three-way catalysts and electronic circuits, were leached in the PDS/NaCl to observe their solubility. Pd and Au were quickly dissolved in the PDS/NaCl solvent. Additionally, 97.18 ± 3.22% of Pd and 99.23 ± 2.18% of Au were dissolved in 300 min. However, Ag, Pt, and Rh were not dissolved in the PDS/NaCl solvent (**Fig. 1d**). Ag was insoluble because of the enormous quantities of Cl^- in PDS/NaCl solvent.[35]. In addition, it was possible that the solvency capability of the PDS/NaCl solvent was insufficient to dissolve Pt and Rh at a temperature of 60 °C and an atmospheric pressure[36].

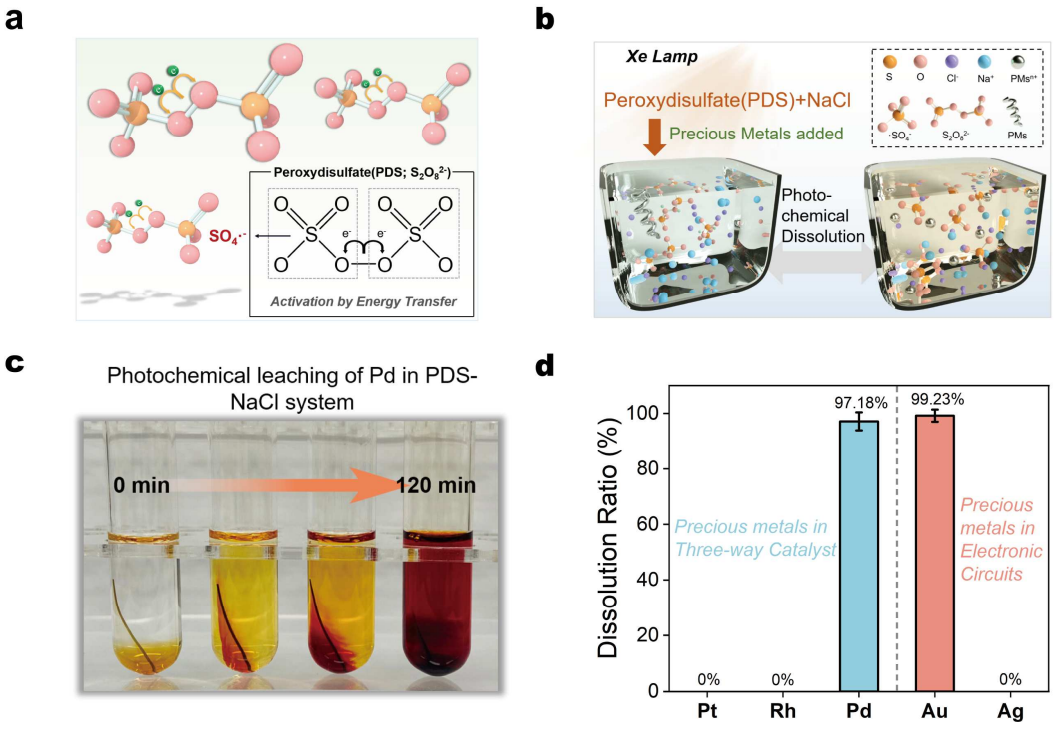

Fig. 1 Photochemical leaching system. a Schematic illustration of the PDS molecular structure.

b Schematic diagram of the leaching of PMs in the mixed solution of PDS and NaCl under Xe lamp light. **c** Dissolved Pd at different leaching times from 0 to 120 min. **d** Dissolution ratios of five common PMs. Reaction conditions: molar ratio of PDS to NaCl=1:1, H_2O add%=70%, mass ratio of salt to metal=100:1, reaction time=300 min, temperature=60 °C.

Leaching experiments of PMs in PDS/NaCl system. As indicated from the initial experiments, Pd and Au could be dissolved in PDS/NaCl solvent. In this section, operating variables including the PDS to NaCl molar ratio, H_2O added, PDS with different chlorinated salts, salt-to-metal mass ratio, temperature, and leaching time were examined to determine the optimal conditions.

As can be seen in **Fig. 2a**, the process of increasing the molar ratios of PDS to NaCl resulted in an increase in the dissolution ratios of both PMs firstly, followed by a decrease process. Pd and Au reached the maximum dissolution ratios and were 96.20 ± 2.58% and 92.13 ± 2.66%, respectively, when the ratio of PDS to NaCl was 1:1. The PMs had different dissolution properties at different PDS to NaCl molar ratios probably due to the different capture effects of Cl^- to $SO_4^{\cdot -}$ and ·OH that produce ·Cl or ·ClOH-[22,37]. As depicted in **Fig. 2b**, as the leaching temperature increased from 20 to 80 °C, the dissolution ratios increased and later diminished. On the one hand, the increasing temperature could improve the activity of the solution and thus enhance the dissolution ratios. On the other hand, excessive temperatures will reduce the activity of free radicals. For instance, the optimal activity of $SO_4^{\cdot -}$ is in the temperature range of 50–70 °C[38]. Therefore, 60 °C was the optimal temperature on comprehensive consideration. **Fig. 2c** showed that, except for $FeCl_2 \cdot 4H_2O$, the other chlorine salts including $ZnCl_2$, $MgCl_2$, $CoCl_3$ and $AlCl_3 \cdot 6H_2O$ with PDS had similar Pd dissolution ratios compared to NaCl. The addition of Fe(II) to PDS turned the solution into a Fenton-like system, promoting the generation of free radicals and thus increased the leaching efficiency of Pd[39]. Other chloride salts did not have a similar effect as $FeCl_2 \cdot 4H_2O$ and only served as the provider of Cl^-. Consequently, the dissolution rates of Pd under these chloride salt systems did not differ too much. Moreover, in the absence of the Xe lamp irradiation, Pd was almost insoluble in PDS/NaCl with only 3.04 ± 0.92% dissolution ratio, indicating that the Xe lamp was a necessary activation method of reactive radicals here[40]. As shown in **Fig. 2d**, the dissolution ratios of Pd and Au were reduced to some extent when the H_2O added increased from 70% to 90%. This was because the intensity of the free radicals generated in the solution possibly decreased

when the H_2O added increased, corresponding to the dilution of the ion concentration. Moreover, as shown in **Fig. 2e**, Pd and Au remained stable dissolution ratios at 240 and 300 min, respectively. So, 240 and 300 min were their individual optimal leaching time. In **Fig. 2f**, when the mass ratio of salt to metal was 100:1, nearly all the metals were leached. As the salt to metal ratio dropped, the dissolution ratios dropped correspondingly. However, the solubility of the two PMs in PDS/NaCl both increased gradually. The solubility of Pd reached 47815 ± 1736 ppm when the salt to metal ratio was 20:1. Nonetheless, the solubility of Au was somewhat lower, which reached 45691 ± 2623 ppm.

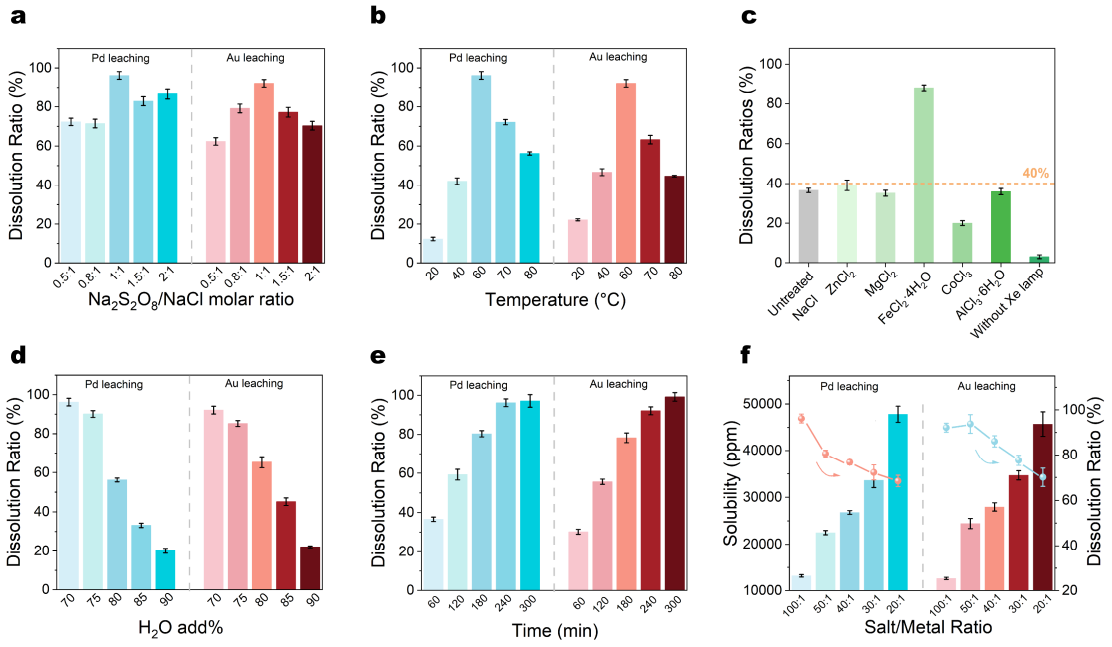

Fig. 2 Dissolution properties of the photochemical system. a-b Dissolution ratios of Pd and Au with varied molar ratios of PDS/NaCl and different temperature. **c** Dissolution of Pd using PDS with different chlorine salts and with or without Xe lamp. **d-e** Dissolution ratios of Pd and Au with varied H_2O added and time. **f** Solubility and dissolution ratios for Pd and Au with different salt to metal mass ratio.

Dissolution mechanism of PMs in PDS/NaCl system. Dissolution rates are significantly impacted by the PM/halide ion coordination mode difference. The dissolution ratio of Pd using the photochemical system was conducted when NaCl was replaced with other sodium halide salts like NaF, NaBr, and NaI. It was found that the dissolution rate of Pd in

PDS/NaBr was faster than that in PDS/NaCl. Next came the PDS/NaI, while Pd was insoluble in PDS/NaF photochemical system (**Fig. 3a**). Due to the varied atomic radii of halide ions, the order of their coordination capacities is $F^- < Cl^- < Br^- < I^-$[36]. Pd was insoluble in PDS/NaF, probably due to the weak complexing ability of F^-. While for NaI system, a large amount of purple smoke was generated when NaI powder were added to aqueous solution of PDS (**Supplementary Fig. S1**), meaning that this solution system would produce a large amount of iodine vapor (I_2), thus reduced the oxidation of the solution. The intensities of $SO_4\cdot^-$ and ·OH in the PDS/NaCl system compared to PDS/NaBr over time were conducted. The PDS/NaCl system had stronger DMPO-$SO_4\cdot^-$ and DMPO-·OH signal intensities (**Fig. 3b** and **Supplementary Fig.S2**). It is probably that the PDS/NaBr system contained more reactive oxygen species other than the radicals. EPR signals (**Supplementary Fig. S3** and **S4)** showed that neither PDS/NaCl nor PDS/NaBr contained $^1O_2$. Moreover, The PDS/NaCl and PDS/NaBr systems were exposed to Xe lamp light for a period, and a moistened starch potassium iodide test strip was placed at the mouth of the bottle to detect the possible formation of chlorine (Cl_2) or bromine (Br_2) vapors. As seen in **Fig. 3c**, the test strip quickly changed color, and a brownish-yellow gas, presumed to be Br_2, was generated at the mouth of the PDS/NaBr solution bottle. Therefore, it is inferred that the PDS/NaBr solution could generate Br_2 monomers as oxidizing active species under Xe lamp light conditions, enhancing the leaching rate of Pd. A similar situation was not present in PDS/NaCl since the test strip at the mouth of the bottle of this solution did not turn blue. This well elucidated the reason for a weaker free radical intensity in the PDS/NaBr system compared to the PDS/NaCl system, while the former had a greater Pd leaching rate.

The results of the free radical quenching experiments were shown in **Fig. 3d**. The methanol (MeOH) was used as $SO_4\cdot^-$ and ·OH scavenger because of the similar reactivity toward $SO_4\cdot^-$ ($k_{SO4\cdot^-+MeOH} = 2.5 \times 10^7 M^{-1}s^{-1}$) and OH ($k_{\cdot OH+MeOH} = 9.7 \times 10^8 M^{-1}s^{-1}$), whereas tert-butanol (TBA) was used to capture the ·OH ($k_{\cdot OH+TBA} = 3.8\text{-}7.6 \times 10^8 M^{-1}s^{-1}$) instead of $SO_4\cdot^-$ ($k_{SO4\cdot^-+TBA} = 4.0\text{-}9.1 \times 10^5 M^{-1}s^{-1}$)[41]. The blank group without any quenching agent had a leaching rate of 96.2 ± 1.95% for Pd at 240 min. The Pd leaching rate after adding 1, 10, and 100 mM of TBA decreased to 83.12 ± 2.73%, 76.27 ± 2.33%, and 68.49 ± 1.41%, respectively. However, the Pd leaching rate plummeted to 5.28 ± 0.36% after adding 100 mM of MeOH, much lower than the group with only ·OH quenching. This suggested that

$SO_4^{\cdot -}$ and ·OH were the principle active species responsible for the oxidative leaching of Pd in the PDS/NaCl system, with $SO_4^{\cdot -}$ making up a higher portion of the total contribution.

Numerous investigations have been carried out regarding the chemical circumstance of PM^{x+} ions in acid and aqueous solutions from both a science and a commercial point of view.[42-44]. In aqueous acidic solutions, previous research indicated that PM^{x+} ions would seemingly form a square-planar framework with four Cl^- and H_2O molecule as coordinating ligands. The ultraviolet–visible (UV–vis) spectroscopy of Pd leaching in the PDS/NaCl solution with varied concentrations were shown in **Fig. 3e**. The firm adsorption peaks at 207 and 237 nm mainly corresponded to the $[PdCl_4]^{2-}$ octahedron[7,45]. It could be inferred that the Xe light excited $SO_4^{\cdot -}$ and ·OH as the oxidation active species in the PDS/NaCl photochemical system to oxidize PMs from PM^0 to PM^{x+}. A large amount of Cl^- in the solution continuously coordinated with PM^{x+} to form complexes, promoting the positive progression of dissolution[46]. The flow of the mechanism of the dissolution process was shown in **Fig. 3f**. The whole process roughly included free radical excitation, oxidative dissolution of PMs, and the coordination process between PM^{x+} and Cl^-.

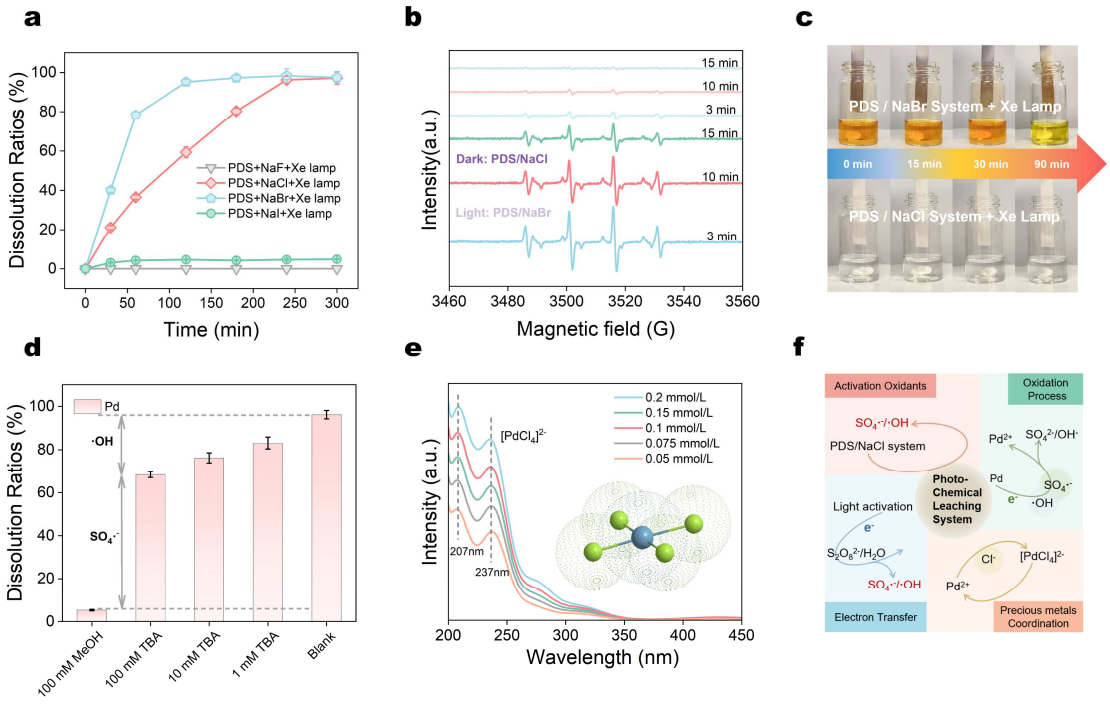

Fig. 3 Dissolution mechanism of PDS/NaCl system. a Dissolution ratios of Pd using PDS with different salts. **b** EPR signal intensity of PDS/NaCl and PDS/NaBr at different times. **c** Discoloration

of starch potassium iodide test strips in PDS/NaCl and PDS/NaBr. **d** Free radical quenching experiment. **e** UV–vis spectra of PDS/NaCl leachate containing Pd(II). **f** The flow of the mechanism of the dissolution process.

Improved leaching system: The PDS/$FeCl_2{\cdot}4H_2O$ Fenton-like system. As seen in the leaching experiments of PMs in PDS/NaCl system section, the efficiency of Pd leaching was significantly improved when NaCl was replaced by $FeCl_2{\cdot}4H_2O$. This phenomenon inspired us to improve the leaching rate of PMs by improving the composition of the leaching system. The effects of the H_2O added and Xe lamp illumination were investigated to explore the efficiency of Pd leaching in the PDS/$FeCl_2{\cdot}4H_2O$ system. The Fenton-like system had the highest Pd leaching rate when 75% of H_2O was added. The decreased ion concentration significantly reduced the Pd leaching efficiency when the H_2O added reached 90%. When 75% H_2O was added, and the Xe lamp was not irradiated, the Pd leaching rate did not differ much (**Fig. 4a**). The dissolution process can be further analyzed by the kinetics experiments. According to eq 1, the dissolution kinetic slope (k_c) of Pd can be calculated as[34]

$$k_c t = 1 - (1 - x)^{1/3} \quad [1]$$

where x represents the Pd dissolution ratio, k_c represents the rate constants (min^{-1}), and t (min) represents the reaction time.

The first-order reaction constants for Pd leaching rates under different experimental conditions were shown in **Fig. 4b**. The reaction constant reached 0.0082 min^{-1} without the Xe lamp irradiation, a very small difference from the optimal condition of 0.097 min^{-1}. The PDS/$FeCl_2{\cdot}4H_2O$ Fenton-like system was an improved PDS/NaCl system. It did not require Xe lamp irradiation, saving a lot of energy consumption and significantly increasing leaching efficiency which took only 90 min to achieve almost 100% dissolution of Pd. In the Fenton-like system, the conversion of Fe^{2+} to Fe^{3+} was the key step affecting the production efficiency of oxidation active species[47]. Therefore, reducing the oxidation of Fe^{2+} may be the key to improve the leaching rate of the PMs. Furthermore, the Pd leaching rates were explored for the change in the molar ratio of PDS to $FeCl_2{\cdot}4H_2O$ and the addition of different ratios of reducing agents, like citric acid (CA), ascorbic acid (AA), and hydrogen peroxide (H_2O_2). As shown in **Fig. 4c**, the Pd leaching effect reached the best leaching effect when the molar ratio of PDS to $FeCl_2{\cdot}4H_2O$ was 1:1. Moreover, adding

reducing agents could improve the leaching efficiency of Pd to a certain extent. AA was the best-reducing agent. The dissolution ratio reached the maximum of 77.31% when the molar ratio of PDS to $FeCl_2 \cdot 4H_2O$ and AA was 1:1 and 10:1, respectively. Fe(II) was analyzed by the 1,10-phenanthroline method. The formed Fe(II)-1,10-phenanthroline complex with a characteristic orange color was measured at 510 nm using a Hach spectrophotometer[48]. Fe_0 represents the total amount of iron ions measured with ICP-OES minus the Fe(II). As shown in **Fig. 4d**, the molar ratio of Fe^{2+} achieved the highest when AA was added, which was consistent with the highest Pd dissolution ratio after adding AA. Several methods, including Hammett acidity[49,50], infrared spectroscopy and etc. [51,52] were used to determine the acidity of the solutions. The Hammett acidity method utilizes UV-vis spectroscopy and can be used to measure the acidity of aqueous and non-aqueous solvents. This technique is user-friendly, requires minimal apparatus, and is highly accurate. The UV–vis absorbance of indicators in PDS/$FeCl_2 \cdot 4H_2O$ solutions with varied percentages of H_2O added was shown in **Fig. 4e**. The Hammett acidity of the PDS/$FeCl_2 \cdot 4H_2O$ solutions with varied H_2O add% was calculated and was listed in **Supplementary Table S1**. The absorbance of the solution and the Hammett acidity decreased as the amount of added H_2O diminished, indicating that the solutions became stronger acids. **Fig.4f** showed the dissolution ratios of Pd and Au in PDS/$FeCl_2 \cdot 4H_2O$ Fenton-like system versus PDS/NaCl photochemical systems in 30 min. PDS/$FeCl_2 \cdot 4H_2O$ solution greatly improved the PMs leaching efficiency and did not require Xe lamp, which made the operation easier and also greatly reduced the energy consumption.

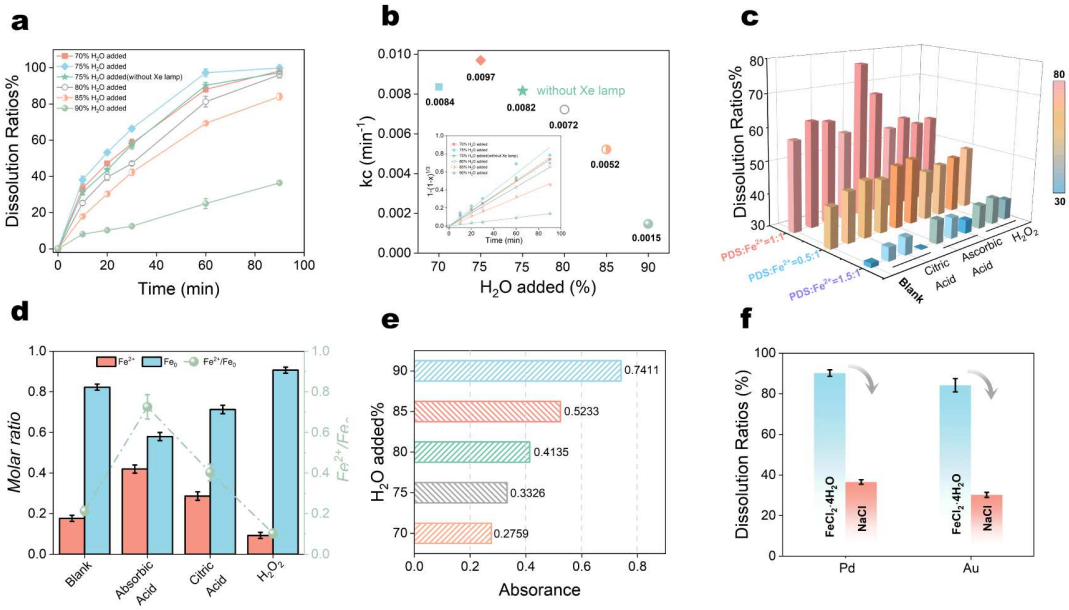

Fig. 4 Dissolution properties of the Fenton-like system. a-b Dissolution ratios and k_c of Pd in PDS/$FeCl_2·4H_2O$ under different conditions. **c** Dissolution ratios of Pd in 30 min with different PDS to $FeCl_2·4H_2O$ ratio and different reducing agents added. **d** Concentrations of Fe^{2+} and Fe_0 for different reducing agents added. **e** Absorbance of PDS/$FeCl_2·4H_2O$ for varied percentages of H_2O added. **f** Dissolution ratios of Pd and Au in PDS/$FeCl_2·4H_2O$ (without Xe lamp) and PDS/NaCl photochemical system.

Dissolution mechanism of PMs in PDS/$FeCl_2·4H_2O$ Fenton-like system. The open circuit potential (OCP) was utilized to evaluate the electron transfer process to elucidate the reaction mechanism between PDS and $FeCl_2·4H_2O$[53]. As shown in **Fig. 5a**, the OCP of the PDS solution remained stable within 70 s, but rose immediately after $FeCl_2·4H_2O$ was added. This indicated a fast transfer of electrons in the PDS/$FeCl_2·4H_2O$ system. Electron transfer helps to generate free radicals and other oxidatively active species[54], which can be identified using other exploration methods.

Identification of the principle reactive species is greatly significant for comprehending the fundamental mechanism of PMs leaching in the PDS/$FeCl_2·4H_2O$ Fenton-like system. EPR techniques were utilized to distinguish the free radicals. As seen in **Fig. 5b**, $SO_4·^-$ and ·OH existed in the PDS/$FeCl_2·4H_2O$ solution, but superoxide radicals ($·O_2^-$) and singlet oxygen ($^1O_2$) did not. Moreover, Fe(IV) had been found in a similar Fenton-like system: Fe(II)/KIO_4 solution[48]. One of the most defining aspects of high-valence metal-oxo species is their ability to engage in oxygen atom exchange (OAE) with water. Therefore,

incorporating ^{18}O isotope into products to confirm the presence of Fe(IV) is essential. Consequently, by using UPLC-Q-TOF MS/MS, the oxidation byproduct of methyl phenyl sulfoxide (PMSO) in the PDS/$FeCl_2{\cdot}4H_2O$ system in $H_2{}^{18}O$ was identified. Considering the slow interaction between Fe(IV) and TBA ($k_{Fe(IV)+TBA} = 6.0 \times 10^1 M^{-1}s^{-1}$), TBA at 100 mM was employed to test for the presence of competing reactive species, specifically $SO_4{\cdot}^-$ and ·OH ($k_{SO4{\cdot}-+TBA} = 4.0–9.1 \times 10^5\ M^{-1}s^{-1}$, $k_{\cdot OH+TBA} = 3.8–7.6 \times 10^8\ M^{-1}s^{-1}$). **Fig. 5c** showed that extracted ion chromatography (EIC) found two signal peaks at m/z = 176.0625 and m/z = 174.0583, which agreed with the estimated m/z of ^{18}O isotope-labeled methyl phenyl sulfone ($PMSO_2$, noted as $PMS^{16}O^{18}O$, m/z = 176.0625 [M-NH_4]) and normalized $PMSO_2$ (noted as $PMS^{16}O^{16}O$, m/z = 174.0583 [M-NH_4]), respectively. Thus, the results demonstrated that ^{18}O was effectively integrated into $PMSO_2$ during PMSO oxidation in the PDS/$FeCl_2{\cdot}4H_2O$ system, confirming that Fe(IV) was generated as a reactive intermediate[55].

Furthermore, the chemical pathways and thermodynamics of the PDS/$FeCl_2{\cdot}4H_2O$ process were thoroughly investigated using density functional theory (DFT) simulations. Subsequently, three possible reaction routes were proposed where $SO_4{\cdot}^-$, ·OH, and Fe(IV) were generated as the reactive species. As shown in **Fig. 5d**, the total energy barrier determined for $SO_4{\cdot}^-$ formation was 7.62 kcal mol^{-1}. However, the total energy barriers for ·OH and Fe(IV) were a bit higher and were 18.46 and 17.52 kcal mol^{-1}, respectively, demonstrating that the formation of high-valent iron was as thermodynamically appealing as those of $SO_4{\cdot}^-$ and ·OH. Additionally, EPR spectroscopy was used to characterize the reactive species produced by the PDS/$FeCl_2{\cdot}4H_2O$ reaction. **Fig. 5e** demonstrated the detection of intense peaks consistent with a DMPO-·OH adduct, which were attributed to the contribution of ·OH and/or Fe(IV) interference by the widely accepted Forrester-Hepburn mechanism[56]. In addition, the EPR signal was studied in the presence and absence of TBA and dimethyl sulfoxide (DMSO) to identify the key intermediate in the creation of the DMPO-·OH adduct. A much lower DMSO concentration (5.0 mM) as the scavenger for both ·OH and Fe(IV) significantly weakened the observed peaks of the DMPO-·OH adduct when compared to the TBA concentration (200 mM), showing that the EPR signal was predominately associated with Fe(IV) and ·OH may function as a secondary intermediate of reactivity for $SO_4{\cdot}^-$ and Fe(IV). Moreover, scavenging experiments supported the EPR test findings. As shown in **Fig. 5f**, TBA reduced the

dissolution ratio of Pd from 98.3 ± 1.13 to 87.53 ± 2.63%, which contributed to the oxidation portion of ·OH in the leaching of Pd. MeOH restrained Pd dissolution to a remarkable degree owing to the notable scavenging impacts of the scavenger on Fe(IV) and both the radicals. Additionally, the Pd dissolution ratio decreased to 31.62% in the DMSO scavenging solution, demonstrating that the contribution of $SO_4{\cdot}^-$ in Pd oxidation was due to the scavenging effects on Fe(IV) and ·OH instead of $SO_4{\cdot}^-$. The schematic illustration of the oxidation dissolution of Pd and Au in PDS/$FeCl_2{\cdot}4H_2O$ by the reactive species $SO_4{\cdot}^-$, ·OH, and Fe(IV) was shown in **Fig. 5g**.

Raman spectroscopy investigation was performed on the Pd(II) containing PDS/$FeCl_2{\cdot}4H_2O$ solution. As shown in **Fig. 5h**, the band at 275 cm^{-1} was observed in both the fitted curves, corresponding to $[PdCl_4]^{2-}$.[45] UV–Vis spectroscopy was not used there because of the interference of Fe^{3+} on the UV signal[57]. Combined with the UV–vis spectra of Pd(II) in the PDS/NaCl filtrate in **Fig. 3e**, it could be inferred that Pd complexes formed the $[PdCl_4]^{2-}$ regular tetrahedron after being oxidized in the PDS/$FeCl_2{\cdot}4H_2O$ system. The dissolution and coordination mechanism of PMs in the PDS/$FeCl_2{\cdot}4H_2O$ solution was shown in **Fig. 5i**. Radicals with high redox potentials (2.60-3.10 V_{NHE} for $SO_4{\cdot}^-/SO_4^{2-}$ and 1.90-2.70 V_{NHE} for $\cdot OH/OH^-$)[58] and Fe(IV) all contributed to the oxidative leaching process. And Fe(IV) may transform to Fe(II) after reducing by PM^{x+}, which enhanced the cycle of Fe(II)[59].

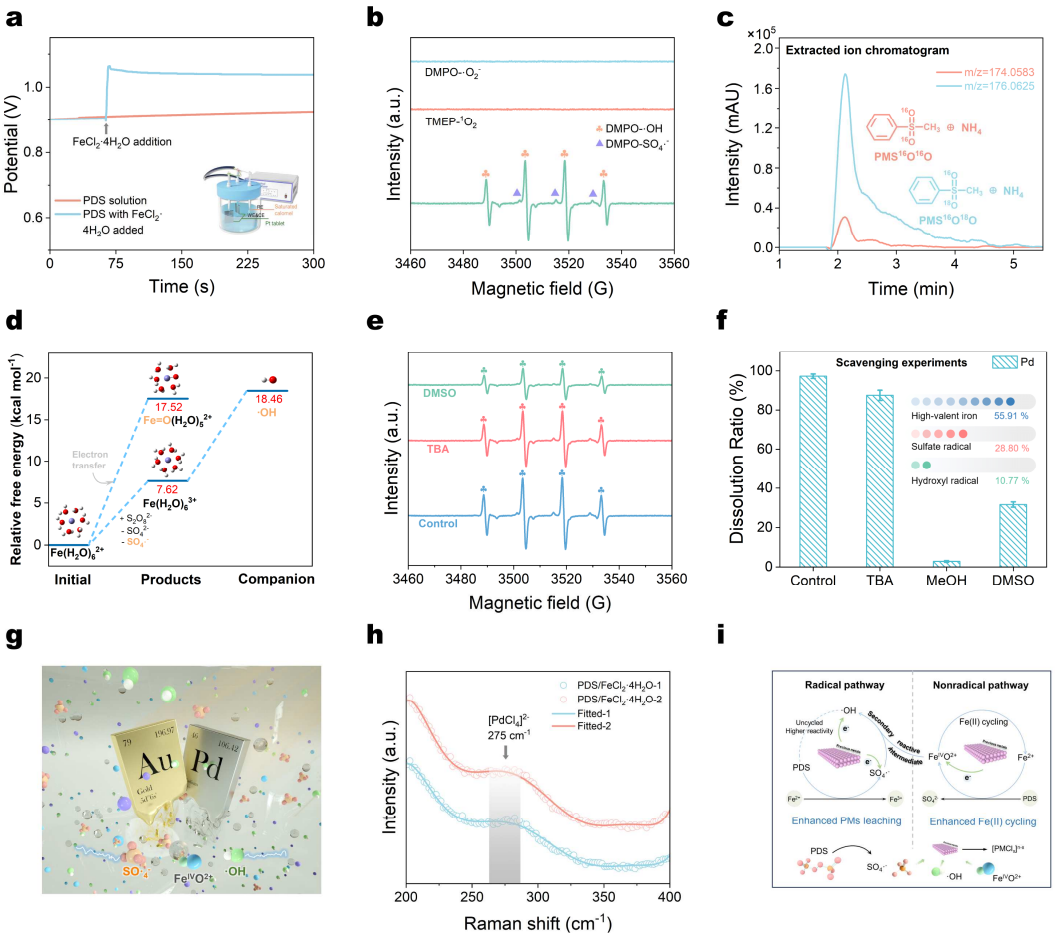

Fig. 5 Dissolution mechanism of PDS/$FeCl_2·4H_2O$ system. **a** OCP curves of the bare PDS solution and PDS after adding $FeCl_2·4H_2O$. **b** EPR spectra of $·O_2^-$, $^1O_2$, ·OH, and $SO_4·^-$. **c** EIC of $PMS^{16}O^{16}O$ and $PMS^{16}O^{18}O$ in PDS/$FeCl_2·4H_2O$ solution with $H_2{}^{18}O$. **d** Free energy relative pathways of the PDS/$FeCl_2·4H_2O$ solution to generate $SO_4·^-$, ·OH, and Fe(IV). **e** EPR spectra in PDS/$FeCl_2·4H_2O$ in the addition of scavengers. **f** Dissolution of Pd in the presence of scavengers in the PDS/$FeCl_2·4H_2O$ solution. **g** Schematic illustration of the oxidation dissolution of Pd and Au in PDS/$FeCl_2·4H_2O$. **h** Raman spectra of Pd(II) in the PDS/$FeCl_2·4H_2O$ solution. **i** Diagram of the dissolution and coordination mechanism of the PMs in the PDS/$FeCl_2·4H_2O$ solution.

Simulated recovery process of PMs. Figure 6a showed the cyclic voltammetry curves at 333 K for the PDS/$FeCl_2·4H_2O$ solution containing Pd(II). Two pairs of oxidation-reduction peaks were observed on the curve, which corresponded to Fe^{3+}/Fe^{2+} and Pd^{2+}/Pd, respectively. The overall simulated recovery process was conducted on PMs wires and their simulated recovery solutions. The Pd wire was first leached in PDS/$FeCl_2·4H_2O$ solution, followed by one-step constant current deposition of 0.02 A

(cathodic) using a three-electrode system. The electric potential curve with electrolysis time (**Fig. 6b**) illustrated that the Pd(II) in leachate decreased from 862.5 ppm to 37.5 ppm after electrodeposition of 3600 s, indicating a high electrodeposition recovery efficiency 95.6%. Eq 7 (**Supplementary**) also calculated the current efficiency, which attained 84.3%.

The energy-dispersive X-ray spectroscopy (EDS) results (**Supplementary Fig. S6-S8**, **Table S5**) indicated that the Pd product was of high purity, and the powder X-ray diffraction (PXRD) pattern confirmed the product's structure (**Fig. 6c**). For the dissolution property, a PDS/$FeCl_2 \cdot 4H_2O$ solution that was regenerated was left to rest. After five cycles of operation, the dissolution ratios and electrodeposition recovery were nearly identical to the initial solution (**Fig. 6d**). **Supplementary Table S7** listed the dissolution ratios, constant current electrolytic recovery and the current efficiency of the electrolysis process for the five simulated cycles of Pd. The recovery method of Au closely resembled that of Pd in a simulated way. 97.3 ± 3.1% of Au was dissolved, with 94.9 ± 1.7% recovered with 1 h at 0.02 A. The current efficiency maintained a high-level and reached 80.1 ± 2.3%. Both the PXRD pattern and EDS results (**Supplementary Fig. S5** and **S9-11**) demonstrated the high purity of the Au product (the chemical composition of elements was listed in **Supplementary Table S6**).

Recovery PMs from spent catalysts. Supplementary Table S8 and **S9** listed the mass composition of two catalysts. The recovery efficiency and purity of Pd and Au were also calculated. More than 98% of the targeted elements in both spent catalysts were dissolved and the Pd and Au recovered after electrodeposition showed a high purity (99.8% for Pd and 99.6% for Au). This technique may be industry-compatible due to the rapid leaching of PMs it produces and the fact that the solution can be recycled. In light of this, we designed a system model for PMs recovery using the PDS/$FeCl_2 \cdot 4H_2O$ solution cycle (**Fig. 6e**). The overall process includes three steps: (1) PDS and $FeCl_2 \cdot 4H_2O$ are added to water to form a Fenton-like system. (2) The spent catalysts are mixed with PDS/$FeCl_2 \cdot 4H_2O$ solution for the leaching. (3) The PM^{x+} are deposition using an electronic device while the solution is recycled into the first step.

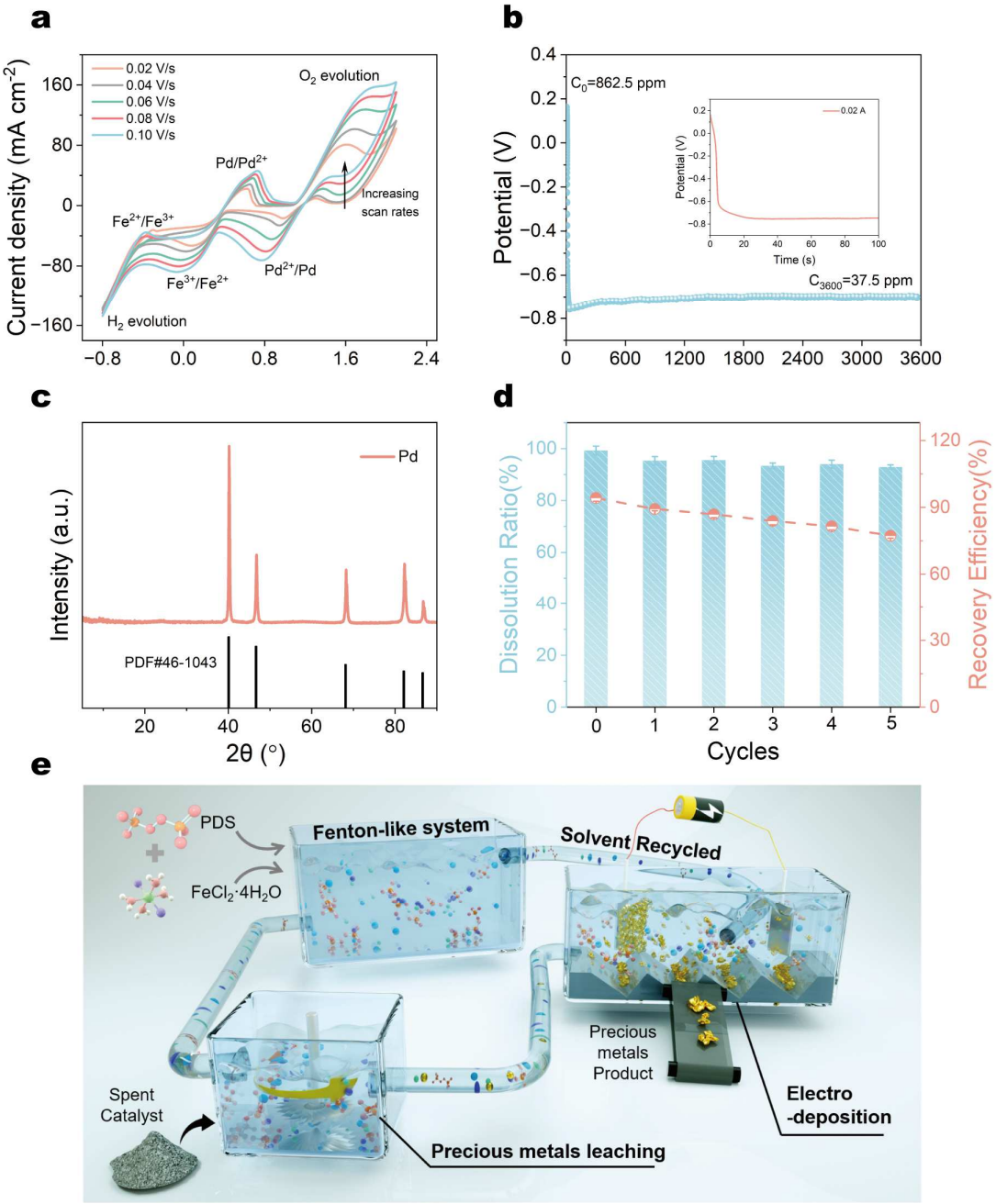

Fig. 6 Recovery process of precious metals. **a** CV curves of Pd(II) in PDS/$FeCl_2 \cdot 4H_2O$. **b** Potential-time curve of Pd(II) in PDS/$FeCl_2 \cdot 4H_2O$. **c** PXRD spectrum of Pd product. **d** Dissolution results of recycled solution. **e** Schematic drawing of the PMs recovery system for industrial applications.

Discussion

Here, we report PDS-based AOPs to develop a novel and simple leaching process for recovering Pd and Au from spent catalysts. The PDS/NaCl photochemical system successfully fully dissolved Pd and Au in 240 and 300 min, respectively. The enhanced PDS/$FeCl_2 \cdot 4H_2O$ Fenton-like system required no Xe lamp light activation and greatly improved the leaching efficiency. Radical identification experiments, ^{18}O Isotope tracing experiments and theoretical calculations proved $SO_4^{\cdot -}$, ·OH and Fe(IV) were the main reactive oxidation species responsible for the leaching process. With solvent leaching and one-step electrodeposition, high-purity precious metals are recovered and the solvent keeps excellent dissolution properties and electrochemical stability after 5 cycles. The whole recovery process does not involve strong acids, toxic cyanide, volatile organic solvents, light activation and any photocatalysts. Because of the rapid leaching of precious metals that it produces and the fact that it can be recycled, this method might be industry compatible. It is anticipated that this research will instigate additional efforts toward the advancement of AOPs technology for resource recycling and that it will open up a green and sustainable method to recover precious metals.

Methods

Radical Identification Experiments. Electro paramagnetic resonance (EPR, Bruker EMX PLUS, German) spectra were collected to identify the intermediate oxidants or radicals generated from the interaction between PDS and $FeCl_2 \cdot 4H_2O$, NaCl or NaBr with DMPO and TEMP as spin-trapping reagent. The EPR spectra were collected under the following conditions: a center field of 3510 Gs, a sweep width of 100 Gs, a static field of 3460 G, a microwave power of 6.325 mV, microwave frequency of 9.85 GHz, modulation frequency of 100 kHz, modulation amplitude of 1.0 Gs and sweep time of 30 s.

Radical Identification Experiments. Radical quenching measurements were conducted to identify the dominant reactive species in PDS/$FeCl_2 \cdot 4H_2O$ or PDS/NaCl systems with MeOH, TBA, DMSO, which were added before the reaction.

Solution Analysis Characterization. The solution analysis characterization of Pd(II) loaded PDS/NaCl and PDS/$FeCl_2 \cdot 4H_2O$ solutions were characterized using an UV-vis-NIR spectrophotometer (UH5300, Hitchi High-Tech Corporation, Japan) and a Raman spectrometer (WITec Alpha, WITec, German) using Zeiss LD EC Epiplan-Neofluar HD Dic 50x/0.55 as the objective lens, respectively.

^{18}O Isotope Tracing Experiments. 1 ml $H_2{}^{18}O$ solution containing 3 mm PMSO, 100 mm TBA was prepared. 0.163 g PDS and 0.137 g $FeCl_2 \cdot 4H_2O$ were added to form the sample after a predetermined time of 15 min, during which the transformation of PMSO was completed. $^{16}O/^{18}O$ isotope-labeled $PMSO_2$ was detected by an ultrahigh-performance liquid chromatography quadrupole time-of flight premier mass spectrometer (UPLC-Q-TOF MS/MS, Waters Co., USA). For the determination of $PMSO_2$, ^{18}O isotope $PMSO_2$ and/or other oxidation products of PMSO in PDS/$FeCl_2 \cdot 4H_2O$ system, a BEH C18 column (100 mm×2.1 mm i.d., 1.7 μm; Waters, Milford, USA) was used. The gradient mobile phase ratio of A/B was set as: the ratio kept at 95/5 for the first 5 min, then changed linearly from 95/5 to 5/95 in the next 15 min and held for 10 min, followed by a sharp decline to 95/5 in 0.1 min, and kept for 10 min for re-equilibration, where A is ultrapure water and B is acetonitrile with the flow rate of 0.15 ml/min. Accurate MS and MS/MS spectra of $PMSO_2$ and/or other products were analyzed in a molecular ion scanning mode (m/z 50 to 600) in negative ESI mode.

Theoretical Calculations. All calculations were performed using the software Gaussian 16[60]. All calculations utilized the PBE0 hybrid functional in conjunction with the D3BJ dispersion correction. For geometry optimization, the mixed basis set (BS1) of def2-SVP for the Fe element and 6-31+G(d) for all other atoms[61], along with the IEFPCM solvent model for water, were employed. Without any structural constraints, the geometries have been completely optimized. Utilizing the SMD continuum solvation model with the larger mixed basis set (BS2) of def2-TZVP for Fe and 6-311+G(d,p) for all other atoms, the final and solvation energies of the fully optimized structures in water were calculated.

Recovering Pd and Au from spent catalysts. We selected waste Pd catalysts for combustion exhaust gas treatment process and waste Au catalysts for methacrolein esterification. In order to assess the metal contents in Pd and Au catalysts, microwave digestion of the waste Pd and Au catalysts was first performed, followed by ICP-OES to test the metal composition in the two catalysts. Then, PDS/$FeCl_2 \cdot 4H_2O$ solution was used to dissolve 1 g Pd and Au catalysts 30 min with a salt to metal ratio of 10:1. After leaching in the solvent, the metal composition in the filtrate was tested. The dissolved PMs were recovered through constant current electrodeposition (0.02 A of cathodic current) for 30 min. After electrodeposition, the Pt sheets of the working electrodes and the PMs product

obtained on the electrodes were microwave digested together and then tested by ICP-OES to calculate the recovery efficiency and purity of the recovered PMs.

References

1 Deng, B. *et al.* Urban mining by flash Joule heating. *Nat Commun* **12**, 5794 (2021).
2 Fu, R. *et al.* Tracing metal footprints via global renewable power value chains. *Nat Commun* **14**, 3703 (2023).
3 Mochizuki, C. *et al.* Defective NiO as a Stabilizer for Au Single-Atom Catalysts. *ACS Catalysis* **12**, 6149-6158 (2022).
4 Sheaffer, K. N. U.S. Geological Survey, Mineral Commodity Summaries. (2023).
5 Doidge, E. D. *et al.* A Simple Primary Amide for the Selective Recovery of Gold from Secondary Resources. *Angew Chem Int Ed Engl* **55**, 12436-12439 (2016).
6 Ding, R. *et al.* Highly Efficient and Selective Gold Recovery Based on Hypercross-Linking and Polyamine-Functionalized Porous Organic Polymers. *ACS Appl Mater Interfaces* **14**, 11803-11812 (2022).
7 Ding, A. *et al.* Salt aqua regia as a green solvent for recovering precious metals. *Cell Reports Physical Science* **3**, 101159 (2022).
8 Yang, L. *et al.* Unveiling the high-activity origin of single-atom iron catalysts for oxygen reduction reaction. *Proc Natl Acad Sci U S A* **115**, 6626-6631 (2018).
9 Asakura, H. *et al.* Fe-Modified CuNi Alloy Catalyst as a Nonprecious Metal Catalyst for Three-Way Catalysis. *Industrial & Engineering Chemistry Research* **59**, 19907-19917 (2020).
10 Chen, Y. *et al.* Selective recovery of precious metals through photocatalysis. *Nature Sustainability* **4**, 618-626 (2021).
11 Nguyen, T. S., Hong, Y., Dogan, N. A. & Yavuz, C. T. Gold Recovery from E-Waste by Porous Porphyrin–Phenazine Network Polymers. *Chemistry of Materials* **32**, 5343-5349 (2020).
12 Li, X. & Binnemans, K. Oxidative Dissolution of Metals in Organic Solvents. *Chemical Reviews* **121**, 4506-4530 (2021).
13 Van den Bossche, A., Rodriguez Rodriguez, N., Riano, S., Dehaen, W. & Binnemans, K. Dissolution behavior of precious metals and selective palladium leaching from spent automotive catalysts by trihalide ionic liquids. *RSC Adv* **11**, 10110-10120 (2021).
14 McGivney, E. *et al.* Biogenic Cyanide Production Promotes Dissolution of Gold Nanoparticles in Soil. *Environ Sci Technol* **53**, 1287-1295 (2019).
15 Birich, A., Stopic, S. & Friedrich, B. Kinetic Investigation and Dissolution Behavior of Cyanide Alternative Gold Leaching Reagents. *Sci Rep* **9**, 7191 (2019).
16 Ahtiainen, R. & Lundström, M. Cyanide-free gold leaching in exceptionally mild chloride solutions. *Journal of Cleaner Production* **234**, 9-17 (2019).
17 Dong, H., Zhao, J., Chen, J., Wu, Y. & Li, B. Recovery of platinum group metals from spent catalysts: A review. *International Journal of Mineral Processing* **145**, 108-113 (2015).
18 Yuan, Z. *et al.* Contact Behavior between Cells and Particles in Bioleaching of Precious Metals from Waste Printed Circuit Boards. *ACS Sustainable Chemistry & Engineering* **6**, 11570-11577 (2018).
19 Lin, W., Zhang, R. W., Jang, S. S., Wong, C. P. & Hong, J. I. "Organic aqua regia"--powerful liquids for dissolving noble metals. *Angew Chem Int Ed Engl* **49**, 7929-7932 (2010).
20 Zhou, Q. *et al.* Generating dual-active species by triple-atom sites through peroxymonosulfate activation for treating micropollutants in complex water. *Proc Natl Acad Sci U S A* **120**, e2300085120 (2023).
21 Zhang, Y. J. *et al.* Distinguishing homogeneous advanced oxidation processes in bulk water from heterogeneous surface reactions in organic oxidation. *Proc Natl Acad Sci U S A* **120**, e2302407120 (2023).

22 Duan, P. *et al.* Effect of phosphate on peroxymonosulfate activation: Accelerating generation of sulfate radical and underlying mechanism. *Applied Catalysis B: Environmental* **298** (2021).

23 Zhu, L. *et al.* Designing 3D-MoS(2) Sponge as Excellent Cocatalysts in Advanced Oxidation Processes for Pollutant Control. *Angew Chem Int Ed Engl* **59**, 13968-13976 (2020).

24 Yang, Z., Cui, Y., Pan, B. & Pignatello, J. J. Peroxymonosulfate Activation by Fe(III)-Picolinate Complexes for Efficient Water Treatment at Circumneutral pH: Fe(III)/Fe(IV) Cycle and Generation of Oxyl Radicals. *Environ Sci Technol*, doi:10.1021/acs.est.3c00777 (2023).

25 Li, R. *et al.* Radical-Involved Photosynthesis of AuCN Oligomers from Au Nanoparticles and Acetonitrile. *Journal of the American Chemical Society* **134**, 18286-18294 (2012).

26 Chen, N. *et al.* Surface-bound radical control rapid organic contaminant degradation through peroxymonosulfate activation by reduced Fe-bearing smectite clays. *J Hazard Mater* **389**, 121819 (2020).

27 Liu, J. *et al.* Ultrasound irritation enhanced heterogeneous activation of peroxymonosulfate with Fe_3O_4 for degradation of azo dye. *Ultrason Sonochem* **34**, 953-959 (2017).

28 Qi, C. *et al.* Activation of peroxymonosulfate by microwave irradiation for degradation of organic contaminants. *Chemical Engineering Journal* **315**, 201-209 (2017).

29 Huang, G. X., Wang, C. Y., Yang, C. W., Guo, P. C. & Yu, H. Q. Degradation of Bisphenol A by Peroxymonosulfate Catalytically Activated with $Mn_{1.8}Fe_{1.2}O_4$ Nanospheres: Synergism between Mn and Fe. *Environ Sci Technol* **51**, 12611-12618 (2017).

30 Wang, J. *et al.* An ultrafast and facile nondestructive strategy to convert various inefficient commercial nanocarbons to highly active Fenton-like catalysts. *Proc Natl Acad Sci U S A* **119** (2022).

31 Wang, R. *et al.* Recycling gold from printed circuit boards gold-plated layer of waste mobile phones in “mild aqua regia” system. *Journal of Cleaner Production* **278** (2021).

32 Firmansyah, M. L., Kubota, F., Yoshida, W. & Goto, M. Application of a Novel Phosphonium-Based Ionic Liquid to the Separation of Platinum Group Metals from Automobile Catalyst Leach Liquor. *Industrial & Engineering Chemistry Research* **58**, 3845-3852 (2019).

33 Li, X., Van den Bossche, A., Vander Hoogerstraete, T. & Binnemans, K. Ionic liquids with trichloride anions for oxidative dissolution of metals and alloys. *Chem Commun* **54**, 475-478, doi:10.1039/c7cc08645h (2018).

34 Zhou, X. *et al.* Unraveling Charge State of Supported Au Single-Atoms during CO Oxidation. *J Am Chem Soc* **140**, 554-557, doi:10.1021/jacs.7b10394 (2018).

35 Yin, Y.-H. & Zhang, L. The structures and properties of (AgCl)n (n= 2–13). *Computational and Theoretical Chemistry* **1097**, 70-78, doi:10.1016/j.comptc.2016.10.013 (2016).

36 Cao, J. *et al.* Aqueous Photocatalytic Recycling of Gold and Palladium from Waste Electronics and Catalysts. *ACS ES&T Engineering* **2**, 1445-1453 (2022).

37 Chen, Y. *et al.* Photocatalytic Dissolution of Precious Metals by TiO_2 through Photogenerated Free Radicals. *Angew Chem Int Ed Engl* **61**, e202213640 (2022).

38 Yang, Q. *et al.* Recent advances in photo-activated sulfate radical-advanced oxidation process (SR-AOP) for refractory organic pollutants removal in water. *Chemical Engineering Journal* **378**, doi:10.1016/j.cej.2019.122149 (2019).

39 Li, L. *et al.* Insights into reactive species generation and organics selective degradation in Fe-based heterogeneous Fenton-like systems: A critical review. *Chemical Engineering Journal* **454** (2023).

40 Chai, L. *et al.* Kinetics and molecular mechanism of arsenite photochemical oxidation based on sulfate radical. *Molecular Catalysis* **438**, 113-120 (2017).

41 Gong, Y. *et al.* MOF-derived nitrogen doped carbon modified g-C3N4 heterostructure composite with enhanced photocatalytic activity for bisphenol A degradation with peroxymonosulfate under visible light irradiation. *Applied Catalysis B: Environmental* **233**, 35-45 (2018).

42 Watanabe, S. *et al.* Spectroscopic and first-principles calculation studies of the chemical

forms of palladium ion in nitric acid solution for development of disposal of high-level radioactive nuclear wastes. *AIP Advances* **8** (2018).

43 Fujii, T. *et al.* Electronic absorption spectra of palladium(II) in concentrated nitric acid solutions. *Journal of Radioanalytical and Nuclear Chemistry* **290**, 475-478 (2011).

44 Purans, J. *et al.* Structural investigation of Pd(II) in concentrated nitric and perchloric acid aolutions by XAFS. *J Phys Chem B* **109**, 11074-11082 (2005).

45 Goggin, P. L. & Mink, J. Vibrational spectra of square-planar tetrahalogeno-gold(III), palladium(II), and platimun(II) anions in solution. *J Chem Soc Dalton Trans*, 1479-1483 (1974).

46 Lommelen, R., Onghena, B. & Binnemans, K. Cation Effect of Chloride Salting Agents on Transition Metal Ion Hydration and Solvent Extraction by the Basic Extractant Methyltrioctylammonium Chloride. *Inorg Chem* **59**, 13442-13452, doi:10.1021/acs.inorgchem.0c01821 (2020).

47 Liu, X., Yan, X., Liu, W., Yan, Q. & Xing, M. Switching of radical and nonradical pathways through the surface defects of Fe_3O_4/MoO_xS_y in a Fenton-like reaction. *Science Bulletin* **68**, 603-612 (2023).

48 Zong, Y. *et al.* Enhanced Oxidation of Organic Contaminants by Iron(II)-Activated Periodate: The Significance of High-Valent Iron-Oxo Species. *Environ Sci Technol* **55**, 7634-7642 (2021).

49 Hao, R., He, J., Zhao, L. & Zhang, Y. HPAs and POM-based ILs Catalyzed Effective Conversion of Furfuryl Alcohol to Alkyl Levulinate. *ChemistrySelect* **2**, 7918-7924 (2017).

50 Ding, A., Liu, C., Zhang, X., Lei, L. & Xiao, C. $ZnCl_2$: A Green Bronsted Acid for Selectively Recovering Rare Earth Elements from Spent NdFeB Permanent Magnets. *Environ Sci Technol* **56**, 4404-4412 (2022).

51 Yang, Y.-l. & Kou, Y. Determination of the Lewis acidity of ionic liquids by means of an IR spectroscopic probe. *Chemical Communications*, 226-227 (2004).

52 Frcaiu, D., Ghenciu, A. & Miller, G. Evalution of acidity of strong acid catalysts I. Derivation of an acidity function from carbon-13 NMR measurements. *J Catal* **134**, 118-125 (1992).

53 Yang, W., Pan, H., Wang, X., Sun, M. & Zhang, Y. Metal-Free Activation of Sulfite by Benzoquinone-Derived Carbon for Efficient Organic Contaminant Degradation: Identification and Regulation of Active Sites. *ACS ES&T Engineering* **3**, 533-543, doi:10.1021/acsestengg.2c00339 (2023).

54 Xing, M. *et al.* Metal Sulfides as Excellent Co-catalysts for H2O2 Decomposition in Advanced Oxidation Processes. *Chem* **4**, 1359-1372, doi:10.1016/j.chempr.2018.03.002 (2018).

55 Wang, Z. *et al.* Further understanding the involvement of Fe(IV) in peroxydisulfate and peroxymonosulfate activation by Fe(II) for oxidative water treatment. *Chemical Engineering Journal* **371**, 842-847, doi:10.1016/j.cej.2019.04.101 (2019).

56 Zong, Y. *et al.* High-valent cobalt-oxo species triggers hydroxyl radical for collaborative environmental decontamination. *Applied Catalysis B: Environmental* **300** (2022).

57 Loures, C. *et al.* Advanced Oxidative Degradation Processes: Fundamentals and Applications. *2035-1755* **5** (2013).

58 Lee, J., von Gunten, U. & Kim, J. H. Persulfate-Based Advanced Oxidation: Critical Assessment of Opportunities and Roadblocks. *Environ Sci Technol* **54**, 3064-3081, doi:10.1021/acs.est.9b07082 (2020).

59 Wang, Z. *et al.* Is Sulfate Radical Really Generated from Peroxydisulfate Activated by Iron(II) for Environmental Decontamination? *Environ Sci Technol* **52**, 11276-11284, doi:10.1021/acs.est.8b02266 (2018).

60 Grimme, S., Ehrlich, S. & Goerigk, L. Effect of the damping function in dispersion corrected density functional theory. *J Comput Chem* **32**, 1456-1465 (2011).

61 Weigend, F. & Ahlrichs, R. Balanced basis sets of split valence, triple zeta valence and quadruple zeta valence quality for H to Rn: Design and assessment of accuracy. *Physical Chemistry Chemical Physics* **7**, 3297-3305 (2005).

Acknowledgments

This work is supported by the National Natural Science Foundation of China (No. U2067213), Natural Science Foundation of Zhejiang Province (LR21B060001) and Science and Technology Program of Institute of Zhejiang University-Quzhou (No. IZQ2021KJ2004).

Author Contributions

C.L.X. designed research; A.T.D., M. L., and C.Y.L. performed research; Q.B.Y. and L.C.L. analyzed data; C.L.X., A.T.D., and M.L. wrote the paper; C.Y.L. supervised the paper.

Competing Interests

The authors declare no competing interest.

Additional information

See more information in Supplementary information.

Supplementary Files

This is a list of supplementary files associated with this preprint. Click to download.

- SupplementalInformation.docx